LASER & PHOTONICS REVIEWS

www.lpr-journal.org

Optical Metasurfaces for Generation and Superposition of Optical Ring Vortex Beams

*Jin Han, Yuttana Intaravanne, Aning Ma, Ruoxing Wang, Songtao Li, Zhancheng Li, Shuqi Chen, Jensen Li, and Xianzhong Chen**

The helical phase structure of a twisted light beam has attracted big interest in both fundamental science and practical applications. A facile metasurface approach to generate and manipulate ring vortex beams is reported and experimentally demonstrated. The generation of ring vortex beams is realized by combining the functionalities of an axicon, a vortex beam generator and a beam deflector onto a single reflective metasurface, which consists of nanorods with spatially variant orientations sitting on a silicon dioxide layer in the middle and a gold layer at the bottom. By controlling the polarization state of the incident light, the superposition of ring vortex beams is continuously tuned. The unique property of the developed device renders this technology very attractive for polarization detection and quantum science related applications.

1. Introduction

It is well known that light can carry two different types of angular momenta, namely, spin angular momentum (SAM) and orbital angular momentum (OAM). SAM can be revealed through the handedness or the polarization of light. Light possessing OAM has a helical wavefront described by $\exp(i\ell\theta)$, where ℓ is the topological charge (TC) of optical vortex (corresponding to an OAM of $\ell\hbar$ per photon) and θ is the azimuthal angle. Recently, the OAM of light has attracted considerable attention as a new degree of freedom in a series of promising applications, such as optical tweezers,[1] multiplexers, and demultiplexers.[2–4] These developments have been triggering a revolution in optical communications based on OAM and SAM. There are many approaches to generating OAM beams, including diffractive optical elements[5] and spatial light modulators.[6] Optical metasurfaces are planar analogy of metamaterials with exotic optical properties, which are able to control light's propagation in a desirable manner.[7–13] The ultrathin nature of optical metasurfaces provides a much compact platform to generate[14] and manipulate OAM beams.[15–18] However, for the mentioned applications in optical communications, usually based on fibers, one needs to match the radial size of the OAM beams (a doughnut shape) to the size of an optical fiber and this strongly depends on the TC of the OAM beam. Recently, Liu et al. have experimentally demonstrated a 3D focused perfect vortex beam, which has a constant radius and is independent of TCs.[19] On the other hand, the superposition of OAM beams can generate novel structure beams,[20–23] for example, the superposition of $\ell = 1$ and $\ell = -1$ can give rise to a vector beam with radially distributed polarization profile, which has been applied in various research fields, including focusing[24] and sensing.[25] However, the superposition of ring OAM beams in the far field has not been studied.

Dr. J. Han, Y. Intaravanne, Dr. A. Ma, R. Wang, Dr. S. Li, Prof. X. Chen
SUPA
Institute of Photonics and Quantum Sciences
School of Engineering and Physical Sciences
Heriot-Watt University
Edinburgh EH14 4AS, UK
E-mail: x.chen@hw.ac.uk

Dr. J. Han
College of Material Science and Engineering
Kunming University of Science and Technology
Kunming 650093, China

Dr. A. Ma
School of Information Science and Engineering
Lanzhou University
Lanzhou 730000, China

R. Wang
Key Laboratory of In-Fiber Integrated Optics of Ministry of Education
College of Physics and Optoelectronic Engineering
Harbin Engineering University
Harbin 150001, China

Dr. S. Li
School of Mathematics and Physics
North China Electric Power University
Baoding 071003, China

Dr. Z. Li, Prof. S. Chen
Laboratory of Weak Light Nonlinear Photonics Ministry of Education
School of Physics and Teda Applied Physics Institute
Nankai University
Tianjin 300071, China

Prof. J. Li
Department of Physics and Center for Metamaterials Research
The Hong Kong University of Science and Technology
Hong Kong, China

The ORCID identification number(s) for the author(s) of this article can be found under https://doi.org/10.1002/lpor.202000146

DOI: 10.1002/lpor.202000146

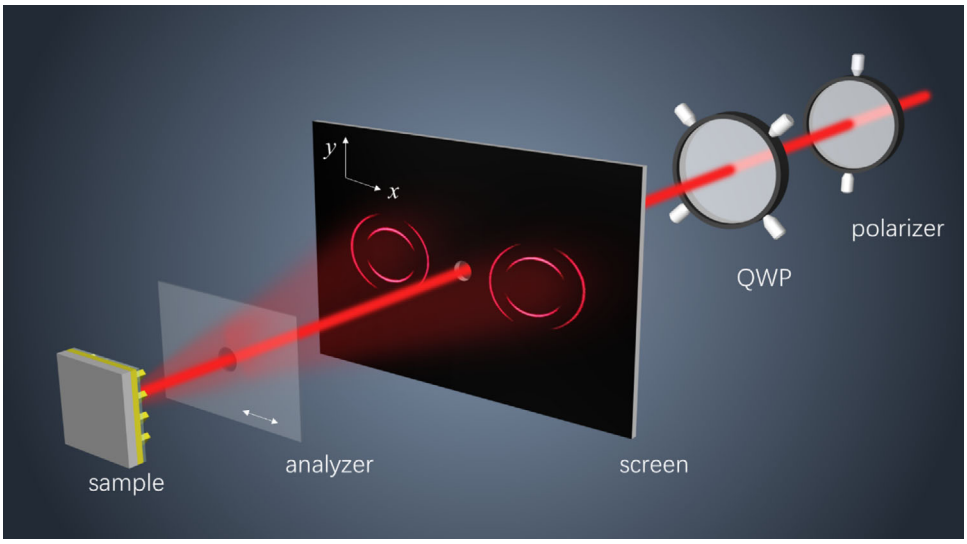

Figure 1. Schematic of the approach for generation and manipulation of ring OAM beams. Incident light with various polarization states is generated by a quarter-wave plate (QWP) and a polarizer. The emitted light from the reflective metasurface generates the superposition of two ring OAM states, which is modulated by passing through an analyzer (linear polarizer) whose transmission axis (white double-headed arrow) is fixed along the horizontal direction. The interference patterns of the superposition of ring OAM beams are displayed on the screen.

In this paper, for the first time we propose and experimentally demonstrate an efficient method to generate the ring OAM beams through a single metasurface, in which the superposition between the generated OAM beams can be continuously tuned by varying the polarization state of the incident light. The speed of such tuning is thus only limited by the external mechanism in changing the polarization of the incident light, rather than by the material tunability of the metasurface itself. Specifically, we combine the functionalities of a vortex beam generator, an axicon and a beam deflector into a single metasurface to generate ring OAM beams. A perfect vortex beam is the Fourier transformation of a Bessel Gaussian beam, which can keep the size of intensity pattern.[19] To generate perfect vortex beams like those in the references,[19,26] a phase profile of spherical wave for a Fourier transform lens with a focal length is necessary. By contrast, the phase term for Fourier transform lens is not needed in our design. Because there is no lens, the resulting ring diameters change with the observation plane at different distances, so that the observation plane far enough away is suitable to see the ring with the naked eyes. Unlike conventional or perfect vortex beams,[26–28] the radius of the ring is only dependent on the axicon period[28,29] and the ring OAM beams in this work can thus be designed to stay constant with different TCs, enabling them to meet with each other and generate superposition for far field observation. As an application example, the superposition of ring OAM beams is used for polarization measurement.

2. Design and Method

Figure 1 shows the schematic of the experimental setup based on an ultrathin metasurface to generate ring OAM states, together with continuous manipulation of their superposition by varying the polarization of the incident light. A polarizer and a quarter wave plate (QWP) are used to control the polarization state of the incident light. The emitted light from the metasurface generates the superposition of ring OAM beams, which is displayed on a screen after passing through an analyzer (linear polarizer), whose transmission axis is fixed along the x direction (see the double-headed arrow in the figure). The screen is a white paper board with an opening (diameter 6 mm) in the middle, which allows the incident light and zero-order reflected light to pass through. In the figure, we also show a typical experimental result of the superposition of ring OAM beams on the screen.

To generate ring OAM beams and realize their superposition, we design two different types of phase profiles based on the combination of phase profiles of a vortex beam generator, an axicon and a beam deflector. $|L,\ell_1\rangle$ and $|R,\ell_2\rangle$ are used to describe a ring OAM state with left circular polarization (LCP) and a TC of ℓ_1 and another ring OAM state with right circular polarization (RCP) and a TC of ℓ_2, respectively. We start from an example to generate a superposition of two ring OAM beams with LCP incidence, the phase profile for the superposition of $|L,\ell_1\rangle$ and $|L,\ell_2\rangle$ on the left side of the screen is governed by

$$\Phi(x,y) = \arg\left(E_1 \exp(i(\ell_1\theta + \Delta\phi_{\text{off}} + \phi_{\text{axicon}})) + E_2 \exp(i(\ell_2\theta + \Delta\phi_{\text{off}} + \phi_{\text{axicon}}))\right) \quad (1)$$

where E_1 and E_2 represent the amplitude components of two ring OAM beams with TCs of ℓ_1 and ℓ_2, respectively. θ is the azimuthal angle and $\Delta\phi_{\text{off}}$ is the phase difference between neighboring pixels to generate a phase gradient along the horizontal (x-) direction, which can realize the off-axis deflection. It is worth mentioning that the off-axis design can avoid the disturbance of the nonconverted part.[22] $\phi_{\text{axicon}}(x,y) = -2\pi\sqrt{x^2+y^2}/d$ is the phase profile for the axicon, where d is the axicon period to control the radius of the generated ring OAM beam.[26,28] The relationship between d and an axicon angle α can be expressed as $d \cdot \sin\alpha = \lambda$, where λ is the wavelength. Details of explanation are

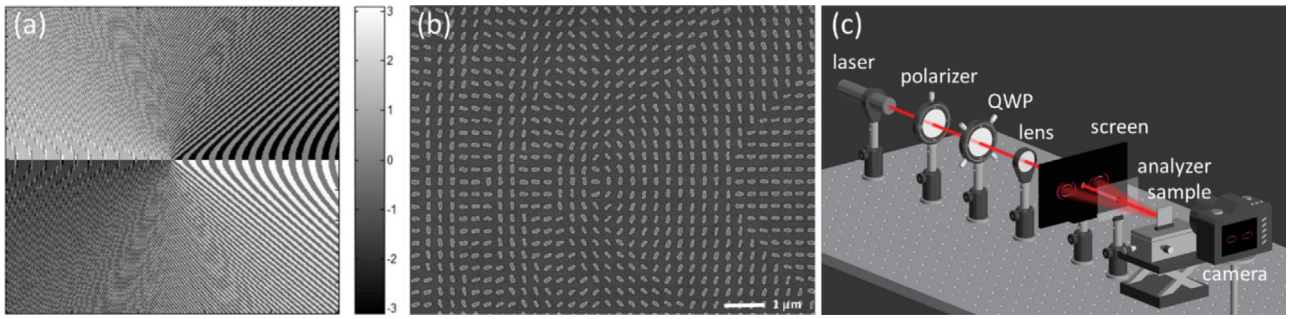

Figure 2. The phase profile used to generate ring OAM beams, scanning electron microscopy (SEM) image of the fabricated sample and schematic of the experimental setup. a) The phase profile to generate ring OAM beams $|L,\ \ell_1 = 1\rangle$ and $|R,\ \ell_2 = -1\rangle$, and the pixel number is 1001 × 1001. b) SEM image of the fabricated metasurface to generate the superposition of two ring OAM beams $|L,\ \ell_1 = 1\rangle$ and $|R,\ \ell_2 = -1\rangle$. The sample has a dimension of 300 μm × 300 μm. Each nanorod functions as a pixel with a size of 300 nm × 300 nm. c) Various polarization states of the incident light with are generated by controlling the angle between the transmission axis of the polarizer and the fast axis of QWP. The light shines on the metasurface at normal incidence and the emitted light from the reflective metasurface is displayed on the screen after passing through an analyzer. The transmission axis of analyzer is fixed along the horizontal.

available in refs. [26 and 28]. In our design, $\Delta\phi_{\text{off}}$ is chosen to be $\pi/5$, corresponding to an off-axis angle of 12.4° at the wavelength of 650 nm. Although larger off-axis angles can be designed, it is not good for our experimental measurement since the collection of high quality photos for images with wider view angle on both sides is more challenging. In addition, the larger off-axis angle can cause image distortion, which is discussed in Section S7 of the Supporting Information. When the incident polarization changes from LCP to RCP, the superposition of $|R,-\ell_2\rangle$ and $|R,-\ell_1\rangle$ is on the right side of the screen since the sign of the generated phase profile is flipped. The superposition of ring OAM beams only occurs when they are on the same ring. There is a slight change in the diameter of the ring (equal to the sample size) on the right side when the incident light polarization is LCP or RCP. Only when the sign of phase for the axicon (plus or minus) is the same, the two ring OAMs have same diameters and can generate superposition. For an elliptical polarization state, there are two different types of superpositions on both sides of the screen.

In order to generate the superpositions of $|L,\ell_1\rangle$ and $|R,-\ell_2\rangle$ on the left side and $|L,\ell_2\rangle$ and $|R,-\ell_1\rangle$ on the right side for any elliptical polarization, the phase profile for LCP incident light is governed by

$$\Phi(x,y) = \arg\left(E_1 \exp(i(\ell_1\theta + \Delta\phi_{\text{off}} + \phi_{\text{axicon}})) + E_2 \exp(i(\ell_2\theta - \Delta\phi_{\text{off}} - \phi_{\text{axicon}}))\right) \quad (2)$$

It should be noted that the superposition does not exist for pure circular polarizations (LCP or RCP) in this case, but it occurs for any elliptical or linear polarization states. Furthermore, the number of displayed dark gaps after passing through the analyzer is determined by $|\ell_1 - \ell_2|$.[19]

Benefiting from high efficiency and broadband, a reflective metasurface is used to experimentally realize such a compact multifunctional device.[30,31] The reflective metasurfaces are composed of three layers, i.e., a top layer of gold nanorods, a silicon dioxide (SiO_2) spacer layer (85 nm), and a gold ground layer (150 nm). All the nanorods have the same geometry and spatially variant orientation angles. Each gold nanorod is 200 nm long, 80 nm wide, and 30 nm thick. The dimension of each pixel is 300 nm × 300 nm. There are 1001 × 1001 pixels in total, meaning that each sample has a dimension of 300 μm × 300 μm. The orientation angle $\varphi(x,y)$ of each gold nanorod is determined by $\varphi(x,y) = \Phi(x,y)/2$.[9] The geometric metasurfaces can generate Pancharatnam–Berry (PB) phase, which is sensitive to circular polarization states.[32] Moreover, the PB phase reverses sign when the incident polarization is changed from LCP to RCP and the phase profile in Equation (1) reverses sign as well.

The designed samples are fabricated using the standard electron beam lithography, followed by film deposition and the lift-off process. Fabrication details are provided in Section S1 of the Supporting Information.

3. Results

A typical polarization state can be described by the major axis of polarization, the ellipticity and handedness (clockwise or counterclockwise). The effect of the major axis of polarization state on the superposition is initially investigated. Based on Equation (2), we first design and fabricate two metasurfaces that can generate the superposition of ring OAM states with TCs of same absolute values and opposite signs (one for $|L,\ \ell_1 = 1\rangle$ and $|R,\ \ell_2 = -1\rangle$ and another for $|L,\ \ell_1 = 2\rangle$ and $|R,\ \ell_2 = -2\rangle$). The phase profile used to generate the superposition of ring OAM beams $|L,\ \ell_1 = 1\rangle$ and $|R,\ \ell_2 = -1\rangle$ is shown in **Figure 2**a. Figure 2b shows the scanning electron microscopy (SEM) image of the fabricated metasurface, which is used to study the relation between the major axis and superposition of ring OAM beams $|L,\ \ell_1 = 1\rangle$ and $|R,\ \ell_2 = -1\rangle$. SEM images of other samples are available in Section S1 of the Supporting Information. The experiment setup to characterize the fabricated metasurface devices is shown in Figure 2c. A tunable laser source (NKT-SuperK EXTREME) is used to generate the desired laser beam with various major axes of polarization states after passing through the polarizer (QWP removed) in front of the sample. A smart phone (HUAWEI Mate20) is used to collect the displayed patterns on the screen after passing through the analyzer whose transmission axis is fixed along the horizontal direction. The distance

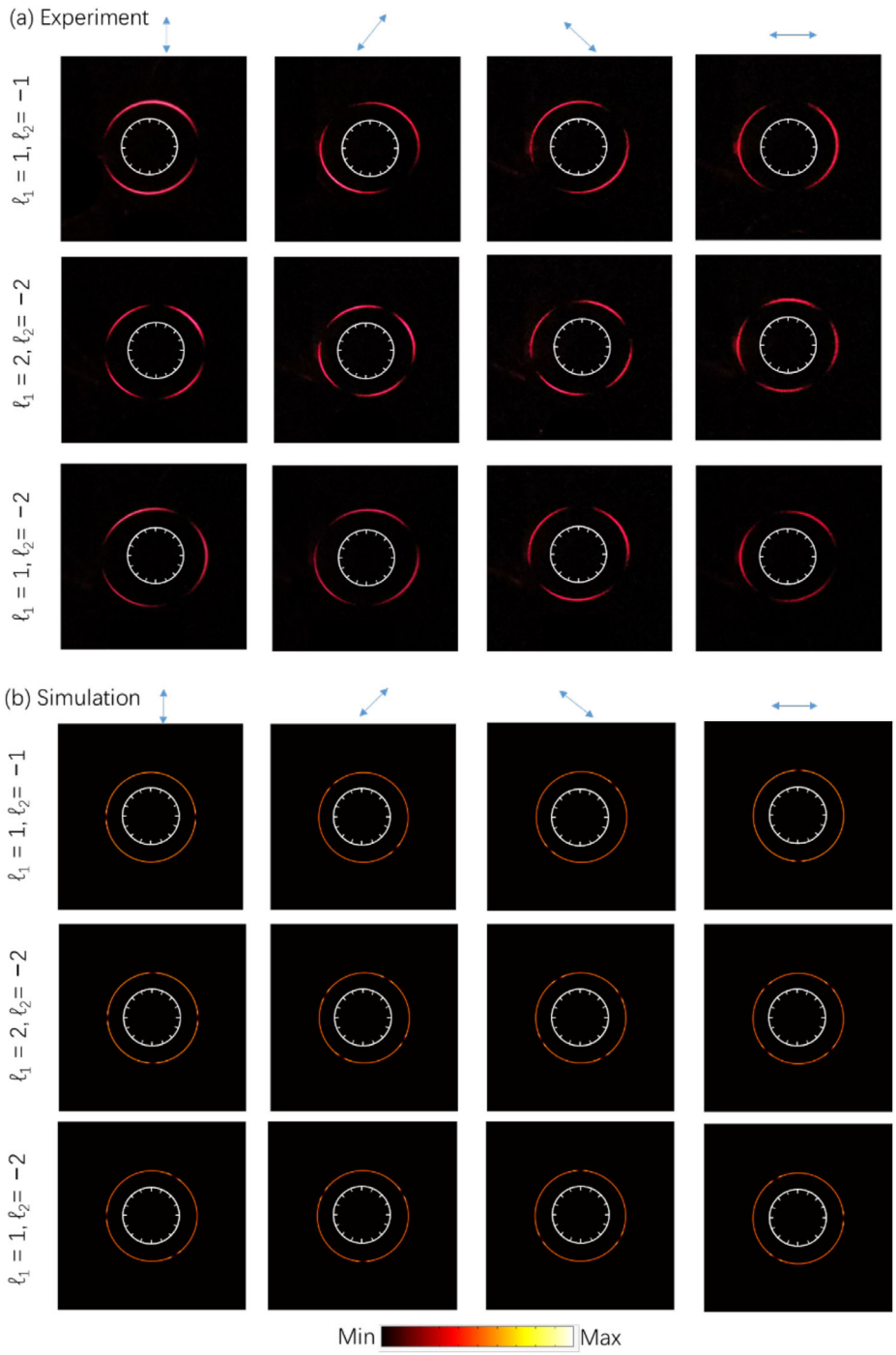

Figure 3. Effect of the major axis of the incident polarization on the superposition of the ring OAM beams. a) Experimental results and b) simulation results for the incident linear light polarization with different major axes (marked with double-headed arrows). The first, second, and third rows in each figure correspond to the superposition of ring OAM beams for $|L, \ell_1 = 1\rangle$ and $|R, \ell_2 = -1\rangle$, $|L, \ell_1 = 2\rangle$ and $|R, \ell_2 = -2\rangle$, and $|L, \ell_1 = 1\rangle$ and $|R, \ell_2 = -2\rangle$, respectively.

between the screen and the metasurface sample is 15 cm. The diameter of ring OAM beams is several centimeters, which can be directly observed with our naked eyes.

There is image distortion since the center of each light beam on one side is not perpendicular to the screen. To solve this issue, we collect the image on one side. By continuously changing the transmission axis of the polarizer, the evolution process of the intensity distribution can be observed, as shown in **Figure 3**. The resultant output beam from the superposition of ring OAM beams $|L, \ell_1 = 1\rangle$ and $|R, \ell_2 = -1\rangle$ with equal components is an

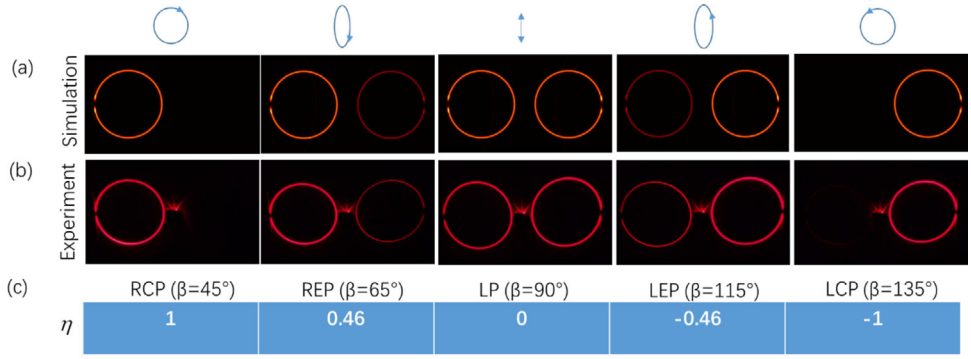

Figure 4. Effects of the ellipticity and the handedness of the incident polarization on the superposition of the ring OAM beams. a) Simulation and b) experimental results for the incident linear light polarization with different ellipticities and the handedness. The evolution process of the intensity change on the two split rings are given when the polarization state of the incident light is changed from RCP to REP, LP, LEP, and LCP. c) The ellipticity and the handedness of the polarized light are described by a parameter $\eta = (1-\sqrt{\tau})/(1+\sqrt{\tau})$, where τ is the ratio of intensity component for LCP to that for RCP. $\eta = \pm 1$ and $\eta = 0$ represent RCP (LCP) and the linear polarization light, respectively. In addition, $\eta > 0$ and $\eta < 0$ correspond to the right elliptical polarization (REP) and left elliptical polarization (LEP), respectively. The values for η in the experiment are given in (c). β is the angle between the transmission axis of the linear polarizer with respect to the horizontal direction.

azimuthally polarized ring vector beam upon the illumination of linearly polarized beam (LP) with a major axis along the vertical direction (see Figure 3a). Although we have $\Delta\phi_{\text{off}}$ destroying the rotational symmetry of the sample in deflecting the superimposed beam to one side, two symmetrically distributed images of red rings with two dark gaps along the horizontal direction are faithfully generated and clearly observed after passing through the analyzer with a transmission axis along the horizontal direction. By gradually rotating the polarization axis of the polarizer from vertical direction to horizontal direction, the azimuthally polarized beam is changed to radially polarized beam, leading to the rotation of two dark gaps on the screen. Furthermore, the rotation angle of gaps is equal to that of the transmission axis of the polarizer with respect to the vertical direction. To facilitate the measurement of major axis, we set a clock dial on the ring. The results for the ring OAM superposition of $|L, \ell_1 = 2\rangle$ and $|R, \ell_2 = -2\rangle$ with equal components are provided in Figure 3b. There are four dark gaps on each light ring and the rotation angle of each gap is halved in comparison with the angle between the transmission axis of the polarizer and the horizontal direction. We can see that the number of gaps in the superposition of ring OAM states $|L, \ell_1\rangle$ and $|R, \ell_2\rangle$ is equal to $|\ell_1 - \ell_2|$. To further confirm the relation between the number of dark gaps and the TCs for the ring OAM superposition, we fabricate a sample to realize the superposition of $|L, \ell_1 = 1\rangle$ and $|R, \ell_2 = -2\rangle$ upon the illumination of LP light. As predicted, three dark gaps are observed in the experimental result (Figure 3). Experimental results for other polarization states are provided in Section S3 of the Supporting Information. The reflective metadevice can work in the broadband, but the diameter of the ring OAM beam increases with the operating wavelength (see Section S5, Supporting Information).

We then study the effect of ellipticity and handedness of the polarization state of the incident light on the superposition of ring OAM beams. We design and fabricate a metasurface that can generate the superposition of ring OAM states with TCs of different absolute values and same signs ($|L, \ell_1 = 1\rangle$ and $|L, \ell_2 = 2\rangle$ for LCP). Suppose the fast axis of QWP is fixed along the vertical direction, five different ellipticities of the polarization states with fixed major axis along the vertical direction can be generated by continuously changing the transmission axis of the polarizer. Only one ring OAM beam is observed on the left or right side of the screen upon the illumination of LCP or RCP light. However, two ring OAM beams can be observed when the incident light is elliptically polarized. When the polarization state is linear polarization, the ring pattern with the same intensity appears on both sides of the screen. The rise and fall of intensities in the ring patterns are closely related to the ellipticity of incident light. It is well known that a completely polarized light is composed of LCP and RCP components. The ellipticity and the handedness of the polarized light can be deduced from the intensity ratio of its LCP and RCP component: $\eta = (1-\sqrt{\tau})/(1+\sqrt{\tau})$, where τ is the ratio of intensity component for LCP to that for RCP. η is changed by controlling the angle between the transmission axis of a linear polarizer and the horizontal direction. Detailed analysis is provided in Section S2 of the Supporting Information. $\eta = \pm 1$ and $\eta = 0$ represent RCP (LCP) and the linear polarization light, respectively. In addition, $\eta > 0$ and $\eta < 0$ correspond to the right elliptical polarization (REP) and left elliptical polarization (LEP), respectively.[33,34] When the resultant beam from the superposition of ring OAM beams passes through the analyzer, two split rings are observed since the uniform light intensity on the rings are modulated. **Figure 4** shows the effect of various ellipticities and handedness on the superposition of ring OAM beam passing through the polarizer. We can clearly see that the intensities on the two split rings change when the polarization state of the incident light is changed from RCP to REP, LP, LEP, and LCP. The dark gap originates from the superpositions of ring OAM beams with different topological charges and same circular polarization states.

4. Discussion

To generate ring OAM beams and manipulate their superpositions, the metasurfaces are designed based on the combination of three different functionalities, i.e., an axicon, a vortex

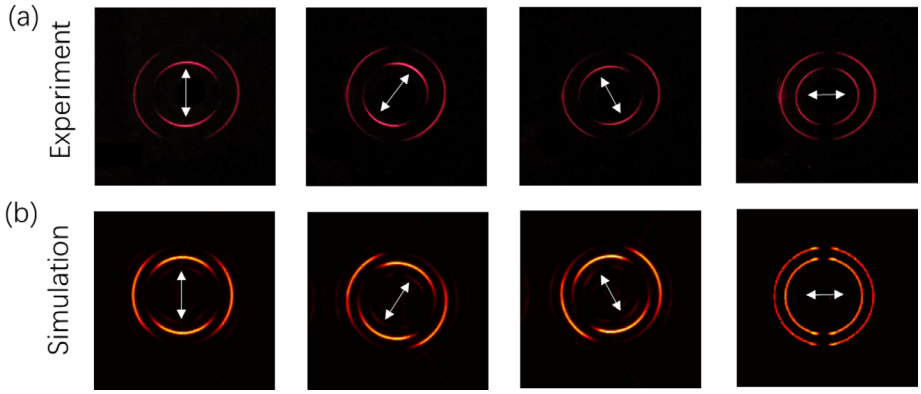

Figure 5. Experimental and simulation results for the measurement of major axis of a polarization state. a) Experimental measurement. b) Simulation results. The measured and expected major axes are marked by the white double-headed arrows in the first and second rows, respectively. The transmission axis of the analyzer is along the horizontal direction.

beam generator, and a deflector. By controlling the major axis, ellipticity, and handedness of the incident polarization state, we have experimentally demonstrated various superpositions of ring OAM beams, whose intensities are spatially modulated after passing through a polarizer. The unusual properties of the developed metasurface devices are very attractive for many research fields, including polarization measurement,[35–38] optical communications, optical tweezers (particle rotation), and quantum sciences.[39,40] As an application example, we experimentally demonstrate polarization measurement based on this new technology. A conventional polarization detection system typically includes many moving optical elements, e.g., polarizers, waveplates, polarization modulators, leading to large volume and high cost.[41] In our measurement, no moving parts are involved. The analyzer has a fixed transmission axis along the *x*-axis. Unlike the polarization measurement based on the metasurface hologram design,[36] our work is based on the integration of an axicon, a vortex beam generator, and a defector.

To simultaneously measure the major axis, ellipticity and handedness of an incident light with an unknown polarization state, we design a compact metasurface device that can generate multiple superpositions of ring OAM beams. The polarization detection is based on two split ring patterns. The inner ring and outer ring are used to detect the major axis and the ellipticity of the incident polarization, respectively. By comparing the intensities on the outer ring on both sides of the screen, one can determine the handedness of the incident polarization. We choose the superposition of $|L, \ell_1 = 1\rangle$ and $|R, \ell_2 = -1\rangle$ for the inner ring and that of $|L, \ell_3 = 1\rangle$ and $|L, \ell_4 = 3\rangle$ for the outer ring. It is worth mentioning that $|\ell_3 - \ell_4|$ does not need to be equal to $|\ell_1 - \ell_2|$. We next quantify the performance of the device. The axicon periods for the inner and outer rings are designed to be $d_1 = 6\ \mu$m and $d_2 = 4\ \mu$m, respectively.

Figure 5 shows the simulation and the experimental results for the measurement of major axis of the polarization state. For the inner ring, no gap is obtained without the analyzer due to the uniform intensity distribution. For the outer ring, a dark gap exists even without the aid of the analyzer. Simulation and experimental results without the analyzer are available in Section S4 of the Supporting Information. If we place the analyzer in front of the screen, a dark gap is observed in the inner ring. The double-headed arrow in the figure shows the major axis of the incident polarization state. The diameters of the inner ring and outer rings are 3.3 and 5.0 cm, respectively. The measured and predicted major axes are given by the white double-headed arrows in the experimental and simulation results, respectively. The existence of dim ring within the designed inner ring is due to the weak coupling between the inner and outer ring OAM beams. Detailed discussion is available in Section S6 of the Supporting Information.

Figure 6 shows the simulation and the experimental results for the measurement of ellipticity and handedness of the incident polarization state. Here, we focus on the detailed change on the outer ring. Although a pair of points on the two rings can work, two symmetrically distributed points can facilitate analysis. To minimize the measurement error, six symmetrically distributed points marked by A and A′, B and B′, C and C′ on the outer rings (shown in Figure 6a) are used to calculate the ellipticity of polarized light. The ellipticity and handedness are determined by rise and fall of intensities on the outer ring on both sides of the screen. The intensities of the outer rings are the same for the incident LP light beam since an LP beam contains the same components of RCP and LCP. Finally, the ellipticities versus the incident polarization (a function of β) are obtained, where β is the angle between the transmission axis of the linear polarizer with respect to the horizontal direction. Good agreement is found between the simulation results (black solid curve) and the experimental measurements (triangles). In our approach, the spin–orbit interaction provided by the metasurface allows coupling from SAM to OAM. It provides a fast and intuitive approach to visualize the polarization state of the incident based on the intensity difference between two split ring patterns. As we discuss above, more accurate polarization information can only be obtained based on the precise measurement and detailed analysis.

5. Conclusion

In a word, we experimentally demonstrate compact metasurface devices to generate ring OAM beams and continuously control their superpositions. Each multifunctional device combines the functionalities of an axicon, a vortex beam generator, and a

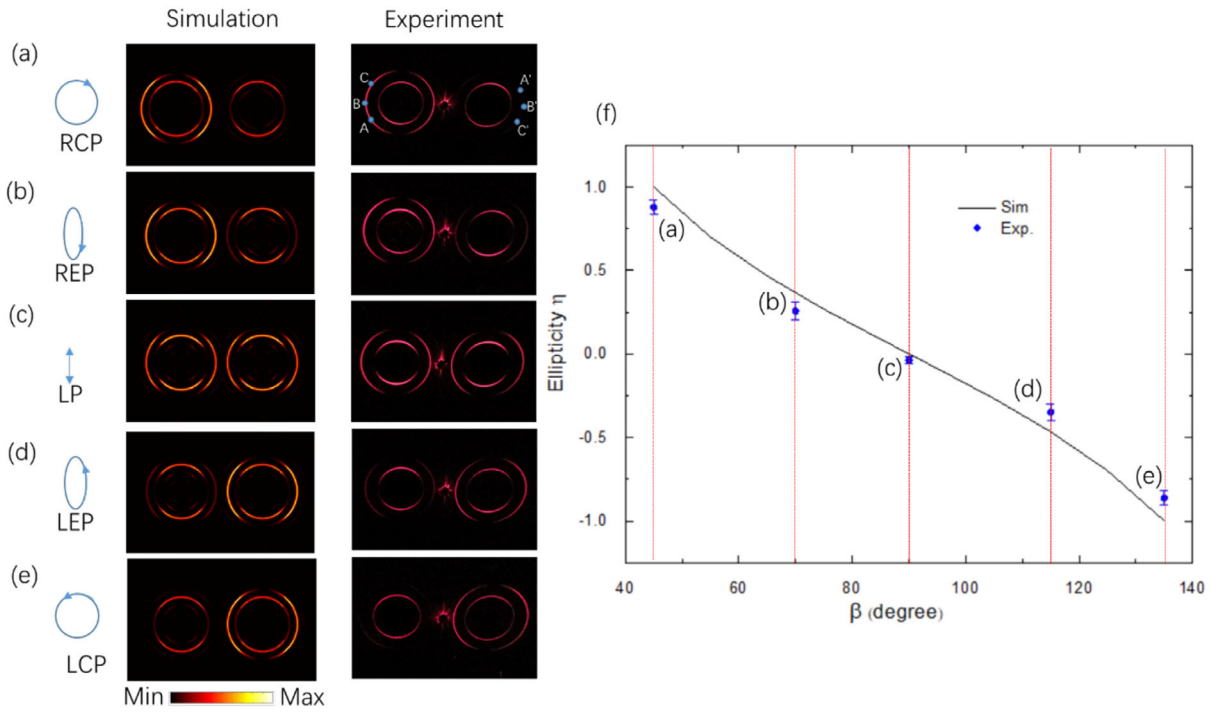

Figure 6. Experimentally measured and simulation results for the measurement of ellipticity and handedness of the incident polarization state. The fast axis of QWP is fixed along the vertical direction. The experimental and simulation results for the superposition of ring OAM beams upon the illumination of incident light with a) RCP, b) REP, c) LP, d) LEP, and e) LCP, which are generated by controlling the angle between the transmission axis of the linear polarizer with respect to the horizontal direction. f) Experimentally measured ellipticities η versus β. β is the angle between the transmission axis of a linear polarizer with respect to the horizontal direction. The solid curve and discreet triangles represent the simulation and experimental results, respectively. Six symmetrically distributed points marked by A and A′, B and B′, C and C′ on the outer rings are used to extract the field intensity. Standard deviation error bars are added.

deflector onto a single device. By controlling the major axis, ellipticity and handedness of the polarization state of the incident light, various superpositions of ring OAM beams are realized. Good agreement between experimental and simulation results is found in the polarization measurement. The compactness, multifunctionality, and robustness render this technology very attractive for polarization detection, optical tweezers, and quantum science related applications.

Supporting Information

Supporting Information is available from the Wiley Online Library or from the author.

Acknowledgements

This project was supported by the Engineering and Physical Sciences Research Council of the United Kingdom (Grant Ref: EP/ P029892/1). Y.I. acknowledges the support from the Ministry of Science and Technology (Thailand), and the Royal Thai Embassy in London (UK). This project was also supported by China Scholarship Council (Grant Nos. 201806185054, 201808535073, 201906680066, and 201906735026). J.L. acknowledges support from the Research Grants Council of Hong Kong (Grant #C6013-18G).

Conflict of Interest

The authors declare no conflict of interest.

6. Author Contributions

J.H. and Y.I. contributed equally to this work. X.C. initiated the idea. J.H., A.M., R.W., S.L., and Z.L. conducted the numerical simulations. Y.I. fabricated the sample. J.H., Y.I., A.M., R.W., and S.L. performed the measurements. J.H., J. L., S.C., and X.C. prepared the manuscript. S.C., J.L., and X.C. supervised the project. All the authors discussed and analyzed the results.

Keywords

optical metasurfaces, orbital angular momentum, ring vortex beams, superposition of ring vortex beams

Received: April 7, 2020
Revised: July 9, 2020
Published online: August 5, 2020

[1] M. Z. Chen, M. Mazilu, Y. Arita, E. M. Wright, K. Dholakia, *Opt. Lett.* **2013**, *38*, 4919.
[2] A. M. Yao, M. J. Padgett, *Adv. Opt. Photonics* **2011**, *3*, 161.
[3] H. Tan, J. H. Deng, R. Z. Zhao, X. Wu, G. X. Li, L. L. Huang, J. Liu, X. L. Cai, *Laser Photonics Rev.* **2019**, *13*, 1800278.
[4] Y. Li, X. Li, L. Chen, M. Pu, J. Jin, M. Hong, X. Luo, *Adv. Opt. Mater.* **2017**, *5*, 1600502.
[5] G. Ruffato, M. Massari, F. Romanato, *Sci. Rep.* **2016**, *6*, 24760.

[6] A. S. Ostrovsky, C. Rickenstorff-Parrao, V. Arrizón, *Opt. Lett.* **2013**, *38*, 534.
[7] N. Yu, P. Genevet, M. A. Kats, F. Aieta, J.-P. Tetienne, F. Capasso, Z. Gaburro, *Science* **2011**, *334*, 333.
[8] S. Sun, Q. He, S. Xiao, Q. Xu, X. Li, L. Zhou, *Nat. Mater.* **2012**, *11*, 426.
[9] X. Chen, L. Huang, H. Mühlenbernd, G. Li, B. Bai, Q. Tan, G. Jin, C. W. Qiu, S. Zhang, T. Zentgraf, *Nat. Commun.* **2012**, *3*, 1198.
[10] W. T. Chen, K. Y. Yang, C. M. Wang, Y. W. Huang, G. Sun, I. D. Chiang, C. Y. Liao, W. L. Hsu, H. T. Lin, S. Sun, L. Zhou, A. Q. Liu, D. P. Tsai, *Nano Lett.* **2014**, *14*, 225.
[11] Z. Zhang, D. Wen, C. Zhang, M. Chen, W. Wang, S. Chen, X. Chen, *ACS Photonics* **2018**, *5*, 1794.
[12] J. Deng, Y. Y, J. Tao, L. Deng, D. Liu, Z. Guan, G. Li, Z. Li, S. Yu, G. Zheng, Z. Li, S. Zhang, *ACS Nano* **2019**, *13*, 9237.
[13] G. H. Yuan, N. I. Zheludev, *Science* **2019**, *364*, 771.
[14] H. Ren, X. Li, Q. Zhang, M. Gu, *Science* **2016**, *352*, 805.
[15] R. C. Devlin, A. Ambrosio, N. A. Rubin, J. P. B. Mueller, F. Capasso, *Science* **2017**, *358*, 896.
[16] Y. Fan, N.-H. S., F. Zhang, Q. Zhao, H. Wu, Q. Fu, Z. Wei, H. Li, C. M. Soukoulis, *ACS Photonics* **2018**, *5*, 1612.
[17] K. Cheng, Z. Wei, Y. Fan, X. Zhang, C. Wu, H. Li, *Adv. Opt. Mater.* **2019**, *7*, 190016.
[18] Z. Li, W. Liu, Z. Li, C. Tang, H. Cheng, J. Li, X. Chen, S. Chen, J. Tian, *Laser Photonics Rev.* **2018**, *12*, 1800164.
[19] Y. Liu, Y. Ke, J. Zhou, Y. Liu, H. Luo, S. Wen, D. Fan, *Sci. Rep.* **2017**, *7*, 44096.
[20] X. Yi, Y. Liu, X. Ling, X. Zhou, Y. Ke, H. Luo, S. Wen, D. Fan, *Phy. Rev. A* **2015**, *91*, 023801.
[21] F. Yue, D. Wen, J. Xin, B. D. Gerardot, J. Li, X. Chen, *ACS Photonics* **2016**, *3*, 1558.
[22] C. Zhang, F. Yue, D. Wen, M. Chen, Z. Zhang, W. Wang, X. Chen, *ACS Photonics* **2017**, *4*, 1906.
[23] F. Yue, D. Wen, C. Zhang, B. D. Gerardot, W. Wang, S. Zhang, X. Chen, *Adv. Mater.* **2017**, *29*, 1603838.
[24] Y. Zhao, J. S. Edgar, G. D. M. Jeffries, D. McGloin, D. T. Chiu, *Phys. Rev. Lett.* **2007**, *99*, 073901.
[25] S. Berg-Johansen, F. Töppel, B. Stiller, P. Banzer, M. Ornigotti, E. Giacobino, G. Leuchs, A. Aiello, C. Marquardt, *Optica* **2015**, *2*, 864.
[26] Y. Zhang, W. Liu, J. Gao, X. Yang, *Adv. Opt. Mater.* **2018**, *6*, 1701228.
[27] M. V. Jabir, N. A. Chaitanya, A. Aadhi, G. K. Samanta, *Sci. Rep.* **2016**, *6*, 21877.
[28] F. Aieta, P. Genevet, M. A. Kats, N. Yu. R. Blanchard, Z. Gaburro, F. Capasso, *Nano Lett.* **2012**, *12*, 4932.
[29] C. Zhang, C. Min, L. Du, X.-C. Yuan, *Appl. Phys. Lett.* **2016**, *108*, 201601.
[30] G. Zheng, H. Mühlenbernd, M. Kenney, G. Li, S. Zhang, *Nat. Nanotechnol.* **2015**, *10*, 308.
[31] C. Zhang, F. Dong, Y. Intaravanne, X. Zang, L. Xu, Z. Song, G. Zheng, W. Wang, W. Chu, X. Chen, *Phys. Rev. Appl.* **2019**, *12*, 034028.
[32] S. Choudhury, U. Guler, A. Shaltout, V. M. Shalaev, A. V. Kildishev, A. Boltasseva, *Adv. Opt. Mater.* **2017**, *5*, 1700196.
[33] L. Huang, X. Chen, B. Bai, Q. Tan, G. Jin, T. Zentgraf, S. Zhang, *Light Sci. Appl.* **2013**, *2*, e70.
[34] D. Wen, F. Yue, S. Kumar, Y. Ma, M. Chen, X. Ren, P. E. Kremer, B. D. Gerardot, M. R. Taghizadeh, G. S. Buller, X. Chen, *Opt. Express* **2015**, *23*, 10272.
[35] J. P. B. Mueller, K. Leosson, F. Capasso, *Optica* **2016**, *3*, 42.
[36] X. Zhang, S. Yang, W. Yue, Q. Xu, C. Tian, X. Zhang, E. Plum, S. Zhang, J. Han, W. Zhang, *Optica* **2019**, *6*, 1190.
[37] A. Pors, M. G. Nielsen, S. I. Bozhevolnyi, *Optica* **2015**, *2*, 716.
[38] F. Yue, V. Aglieri, R. Piccoli, R. Macaluso, A. Toma, R. Morandotti, L. Razzari, *Adv. Mater. Technol.* **2020**, *5*, 1901008.
[39] K. Wang, J. G. Titchener, S. S. Kruk, L. Xu, H. Chung, M. Parry, I. I. Kravchenko, Y. Chen, A. S. Solntsev, Y. S. Kivshar, D. N. Neshev, A. A. Sukhorukov, *Science* **2018**, *361*, 1104.
[40] P. Georgi, M. Massaro, K. Luo, B. Sain, N. Montaut, H. Herrmann, T. Weiss, G. Li, C. Silberhorn, T. Zentgraf, *Light Sci. Appl.* **2019**, *8*, 70.
[41] E. Compain, B. Drevillon, *Appl. Opt.* **1998**, *37*, 5938.